ELSEVIER

Contents lists available at ScienceDirect

## Sensors and Actuators Reports

journal homepage: www.sciencedirect.com/journal/sensors-and-actuators-reports





# Complementary square wave voltammetry and tandem mass spectrometry analysis to identify and detect compensatory genomic changes in nematodes due to nickel (II) exposure

Elizabeth R. LaFave, Ryne Turner, Nicholas J. Schaaf, Thekra Hindi, David Rudel, Eli G. Hvastkovs \*

Department of Chemistry, 300 Science and Technology Building, East Carolina University, Greenville NC 27858, United States

#### ARTICLE INFO

Keywords: SWV analysis LC-MS/MS DNA damage Nematode DNA 8-oxo-Guanine

#### ABSTRACT

Nickel is a toxic heavy metal that may cause negative health outcomes including cancer upon exposure [1]. Square wave voltammetry was used to assay DNA directly extracted from nickel-exposed nematodes that had originated from either high or low Ni-containing environments in order to assess the role of evolutionary genetics in the Ni toxicity process. Extracted DNA was immobilized on pyrolytic graphite (PG) electrodes following layer by layer (LbL) protocols and then electrochemically oxidized in the presence of Ru(bpy)<sup>3+</sup> to generate electrocatalytic oxidative currents at  $\sim +1.05$  V vs. SCE. Both C. elegans and P. pacificus nematodes were utilized, each with a volcanic or cosmopolitan soil source strain. DNA oxidative peak currents (I<sub>D</sub>) increased for all nematode strains upon exposure to 50  $\mu$ g/L Ni<sup>2+</sup>, but those originating from volcanic soils exhibited significantly (40–50%) lower I<sub>p</sub> upon Ni<sup>2+</sup> exposure compared to similarly exposed nematodes from cosmopolitan soils. Further SWV analysis was performed on DNA from a series of C. elegans N2xCB4856 recombinant inbred advanced intercross line populations (RIALs). A continuum of  $I_p$  magnitude was seen as a function of  $Ni^{2+}$  exposure among the RIAL strains indicating Ni-tolerance is complex and affected by multiple loci. The majority of the DNA from Ni-exposed individual RIAL strain cultures produced an increase in oxidative current in comparison to DNA from analogous Ni-unexposed cultures of the same RIAL strains. Liquid chromatography tandem mass spectrometry (LC-MS/MS) analysis on acid hydrolyzed nematode DNA provided validation of the electrochemical findings. Guanine and oxidatively damaged guanine content were monitored via appropriate m/z mass transitions. Guanine content in all Ni-exposed RIAL DNA was lower, while oxidatively damaged guanine was elevated compared to unexposed nematodes in all but one analyzed RIAL. Combined, the complementary electrochemical and MS/MS data provide evidence that evolutionary genetics leads to genetic protection from environmental toxicants, suggesting a possibility that multiple genes are involved in the protection of the organism from Ni exposure.

#### 1. Introduction

The presence of nickel (Ni) in the environment is necessary for the health and survival of many plants and microbes, and it is introduced to the environment naturally via volcanic activity and weathering. Human influences such as mining and metallurgy, however, have caused a significant increase of Ni to be deposited throughout the environment, which in turn causes increased concentrations of this heavy metal to be deposited in soils and waterways [1–3]. The accumulation of Ni by plants and lower order organisms as well as direct intake through breathing and drinking of particulate matter can result in the eventual

increased exposure of this metal to humans and animals [1], which may not be well equipped to deal with the resultant toxic effects [3].

Human exposure to Ni often results in allergic skin reactions, but it has also been linked to respiratory illness and cancer in extreme cases [1]. Humans are often exposed to Ni in the form of jewelry, metallic clothing additions, or even metallic phone cases[4]. However, environmental Ni exposure can arise via different means based on the exposure medium and other environmental parameters [5–12]. Insoluble or particulate Ni forms have been shown to exhibit elevated toxicity compared to soluble forms resulting in post-translational histone modifications in rats [11]. The elevated toxicity may be due to continual

E-mail address: hvastkovse@ecu.edu (E.G. Hvastkovs).

<sup>\*</sup> Corresponding author.

Ni<sup>2+</sup> release once taken into cells [13]. Soluble Ni<sup>2+</sup> exposure has also been linked to both survivorship and fecundity decreases in a concentration dependent manner using a nematode model organism [1].

Nematode species Caenorhabditis elegans and Pristionchus pacificus are often used as inexpensive eukaryotic models to study the effects of environmental toxins. Nematodes have been found in a wide range of environmental conditions, allowing for the study of myriad survival mechanisms and the potential of inherited traits [14-16]. Biological assays to search for potential genetic damage are used to monitor these impacts. Cell death assays are often used to monitor these impacts as genotoxicity caused by toxin exposure can result in apoptosis. Programmed cell death (PCD) is induced in the presence of severe DNA damage to avoid negative impacts to the organism overall [17-20]. PCD assays often employ dyes or green fluorescent protein (gfp)-modified transgenic nematode lines where apoptosis in germline cells results in dye marking or in a halo-like sheath engulfment formation from the transgenic protein that can be visualized and quantified using fluorescent microscopic techniques. We previously used this assay to show how Ni<sup>2+</sup> exposure causes DNA damage, which initiates apoptosis in the nematodes [21].

The drawback to this assay is the necessity of the properly modified organism, the time necessary to count the PCD formations, and the lack of sensitivity to detect apoptotic events from low concentration toxicant exposures. To remedy some of these drawbacks, we reported an electrochemical assay to detect damage or mutational content changes rapidly and sensitively from DNA extracted from living organisms [21, 22]. DNA extracted from Ni-exposed C. elegans nematodes was immobilized using layer by layer (LbL) techniques and oxidized using square wave voltammetry (SWV) in the presence of ruthenium trisbipyridine  $(Ru(bpy)_3^{2+})$  [21–25]. Oxidation of DNA in the presence of the ruthenium metal catalyst at  $\sim$ 1.05 V vs. SCE produced higher electrocatalytic peak currents  $(I_p)$  as  $Ni^{2+}$  concentration increased suggesting higher DNA damage amounts due to the Ni exposure. These data mirrored the dye and gfp-PCD assays, which showed that Ni<sup>2+</sup> caused DNA damage; however the electrochemical detection approach was significantly more sensitive allowing detection of DNA changes at significantly lower Ni exposure concentrations [21].

Here, we build on this previous report and turn to studying animals originating from different Ni-containing environments. First, we electrochemically monitored DNA samples extracted from either C. elegans or *P. pacificus* species that had either been unexposed or exposed to Ni<sup>2+</sup>. Within each species, one strain was sourced from a cosmopolitan soil containing very little Ni content and one was sourced from volcanic soil known to contain elevated amounts of Ni. We also obtained recombinant inbred advanced intercross lines (RIALs) generated from these strains [26-28]. The purpose here was to determine if evolutionary considerations based upon environmental factors influence the DNA damage accumulated from Ni exposure, and then attempt to determine if the electrochemical assay could identify genetically modified organisms exhibiting varied protection to Ni insult. Finally, we validated our electrochemical assay findings using previously reported complementary tandem mass spectrometry (MS/MS) techniques [22] to show that both guanine and damaged guanine (8-oxo-guanine, 8oxoG) content change based on genetic strain and Ni exposure. Overall, the electrochemical SWV and LC-MS/MS complementary approaches here can be used to provide valuable insight into a complicated environmental and evolutionary genetic process.

## 2. Materials and methods

#### 2.1. Materials

Tris buffer was from Fluka, poly(diallyldimethylammonium chloride) (PDDA), poly(sodium 4-styrenesulfonate) (PSS), and tris(2,2′-bipyridyl)dichlororuthenium (Ru(bpy)<sub>3</sub><sup>2+</sup>), formic acid, iron (II) chloride, nickel (II) chloride, hydrogen peroxide, acetonitrile, methanol

(HPLC Grade), ethanol, phenol and chloroform were from Sigma. Calf thymus DNA (sodium salt) was from Calbiochem. Purified 18 M $\Omega$  DI water was generated using a Siemens high-purity water system. All other chemicals for the electrochemical experiments were from Sigma and were reagent grade.

C. elegans nematode strains N2 and CB4856 (CB) and P. pacificus nematode strains PS312 (PS) and RS5696 (RS) were used [1]. N2 is a C. elegans wild-type strain originally found in England. CB4856 is a C. elegans strain sourced from volcanic soil in Hawaii. PS312 is a P. pacificus strain sourced from Pasadena Botanical Gardens in Pasadena, California. RS5696 is a P. pacificus strain sourced from volcanic soil in New Zealand.

RIALs were bred using a nickel resistant strain (CB4856) and a non-resistant nickel strain (N2) [28]. N2 animals were bred with CB4857 animals, and the hybrid heterozygous F2 progeny were individually isolated; single animals were used to start new cultures. This isolation was performed for 10 sequential generations for each singled F2 resulting in each giving rise to a unique strain with a unique combination of heterozygote alleles from the starting populations. Each RIAL has its own strain designation to distinguish it from the other strains with different gene combinations (Table S1).

#### 2.2. Nematode cultures and harvesting

Nematodes were grown on K-media agar plates seeded with *Escherichia coli*, strain OP50. Nematodes were grown on 3 large K-media agar plates with and without nickel at 20 °C until the plate became visibly food limited but not starved. Plates without nickel grew for 5 days to a full culture, while plates containing nickel needed 6 or 7 days to obtain a dense enough culture for harvesting. These plates were then washed using phosphate-buffered saline (PBS) and transferred to a 15 mL conical tube. The tube was centrifuged at 2000 rpms for 5 min, and the supernatant discarded leaving a pellet of worms. 3 mL additional PBS was pipetted into the conical tube with the nematodes, followed by washing by inversion and again centrifuged. This was repeated until the supernatant appeared clear of foggy bacterial contamination. 1 mL of worm lysis buffer was then added to the Falcon tube prior to freezing.

#### 2.3. DNA extraction

After thawing the pellet, 100 µl of proteinase K at a concentration of 1 mg mL<sup>-1</sup> was added and then placed in a shaking incubator at 55 °C for 2 h, and then repeated. After the second incubation, the Falcon tube was heated to 95 °C for 10 min and then placed on ice. 2 µl of RNAse A was added and the solution was placed in the shaking incubator at 37  $^{\circ}$ C for 30 min and repeated. 1 mL 50:50 tris saturated phenol (pH 8): chloroform mixture was added directly to the supernatant and mixed. The solution was then centrifuged at 2000 rpm for 5 min. The top layer was decanted to a new tube and the phenol: chloroform step was repeated twice. This was followed by 3 separate washes of 1 mL chloroform. After the last chloroform wash, the top aqueous layer, containing the DNA, was placed in a new tube and approximately 1/10 vol of 5 M NaCl solution was added followed by the addition of two equivalents of ice-cold ethanol prior to gentle mixing. The ethanol solution was placed in the freezer for storage and to allow precipitation of genomic DNA.

The genomic DNA in ethanol was centrifuged at 4000 rpm for 15 min, followed by decanting of ethanol from the pellet. The pellet was then washed with 2 ml of 70% ethanol and again centrifuged at 4000 rpm for 10 min followed by ethanol decanting. The pellet was air-dried until the outside of the pellet appeared clear but the inner core remained lightly cloudy. 75  $\mu l$  of distilled water was added and the tube was left to settle at 4 °C. After solubilization of DNA, it was centrifuged at 4000 rpm for 10 min to pellet insoluble material. The concentration of soluble nucleic acid was determined using a Thermo Nanodrop and quality ensured using an ethidium bromide stained agarose gel alongside 1 kb

ladder standards.

#### 2.4. Electrode preparation

Pyrolytic graphite (PG, McMaster-Carr (Elmhurst, IL) source) electrodes (2 mm dia.) were manufactured in-house and abraded on 800 grit SiC (Buehler) paper followed by rinsing and sonication in DI  $\rm H_2O$ . After drying under an argon stream, the electrodes were then exposed to the following solutions: PDDA (30  $\mu L$  droplet, 3 mg mL $^{-1}$  in DI  $\rm H_2O$  with 50 mM NaCl) for 15 min followed by PSS (3 mg mL $^{-1}$  in DI  $\rm H_2O$  with 50 mM NaCl). These steps were repeated twice. DNA was applied from solutions 0.100 mg mL $^{-1}$  in 10 mM Tris, pH 7.4 (initial analysis, Fig. 1) or 0.100 mg mL $^{-1}$  in 10 mM Tris + 50 mM NaCl, pH 7.4 (RIAL DNA) for 30 min substituting for PSS in the following rounds. The electrode was rinsed with DI water between each layer. The final film formation for the electrodes was (PDDA/PSS)<sub>2</sub>(PDDA/DNA)<sub>2</sub>.

#### 2.5. Electrochemical measurements

All electrochemical measurements were performed using a CH Instruments (Austin, TX) Model 660A potentiostat. Modified electrodes were placed in a standard three-electrode electrochemical cell (Pt counter, saturated calomel (saturated KCl) reference in 10 mL buffer (10 mM tris, 10 mM NaCl, pH 7.4) with 50  $\mu$ M Ru(bpy)3 $^{2+}$ . Square-wave voltammograms (SWV) were obtained using the following parameters: scan from 0 to +1.3 V, 15 Hz frequency, 4 mV step height, 25 mV amplitude.

#### 2.6. LC-MS DNA preparation

Nematode DNA samples (0.100 mg mL-1) were diluted in equal volume in 44% formic acid followed by heating for 1 h at 120 °C in 1 mL vacuum hydrolysis tubes. The solutions were then transferred to Amicon Ultra-0.5 mL 3 K filter tubes and centrifuged for 40 min at 30,000 x g. The filtrate was then transferred to LC vials containing 10  $\mu$ L inserts. For standard addition analysis, following hydrolysis, 1.0 nmol guanine

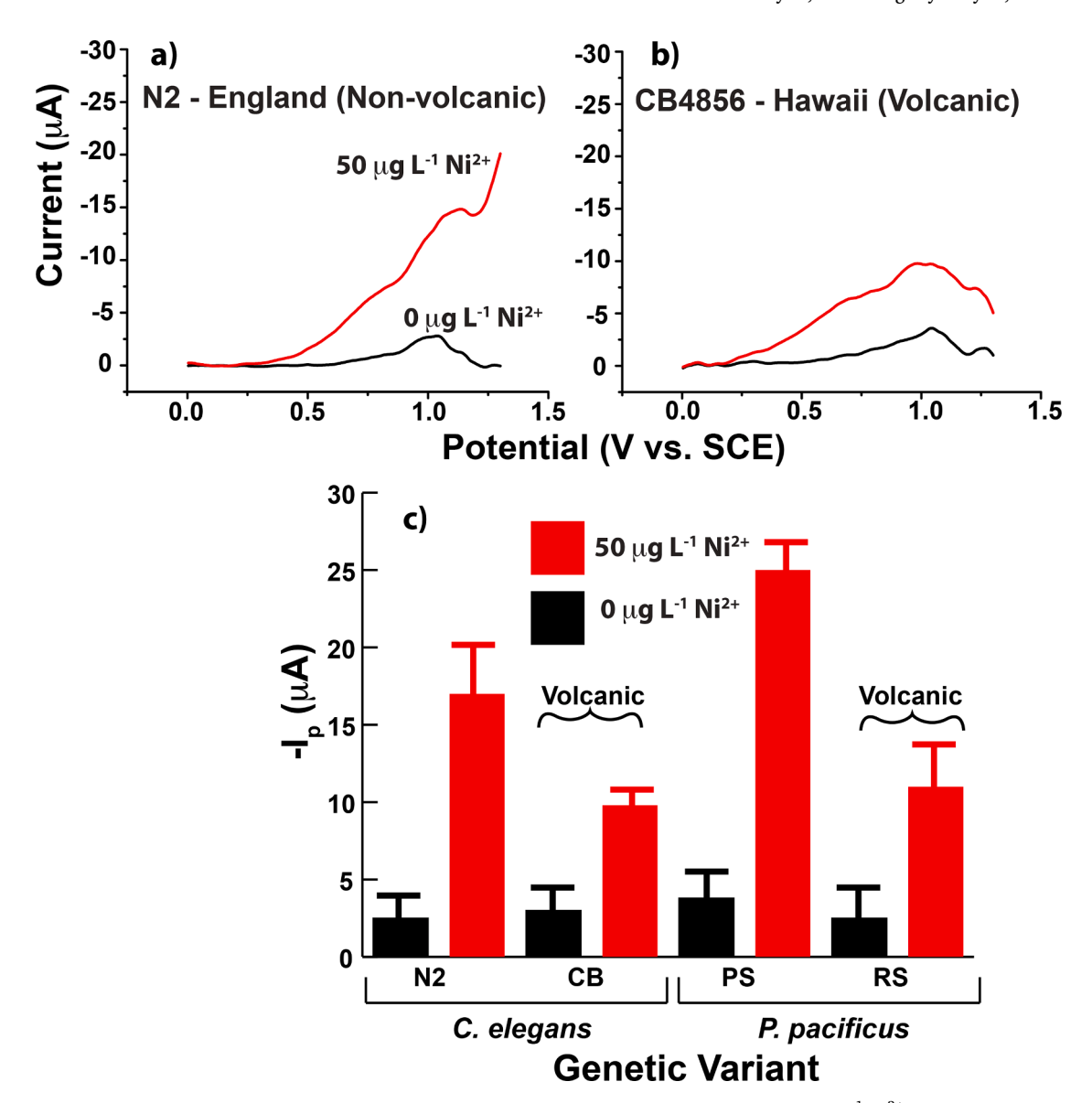


Fig. 1. *C. elegans* DNA background subtracted SWV comparison showing representative unexposed (black) or 50  $\mu$ g L<sup>-1</sup> Ni<sup>2+</sup> exposed (red) responses. DNA was extracted from nematodes originating from a) non-volcanic (N2) or b) volcanic (CB4856) soil environments. c) Average peak current ( $I_p$ , n=3) obtained from *C. elegans* and *P. pacificus* nematodes originating from non-volcanic or volcanic soil environments. Black shows unexposed and red shows DNA from nematodes exposed to 50  $\mu$ g L<sup>-1</sup> Ni<sup>2+</sup>.

standard was added before filtration. Following the aforementioned filtration steps, the solution was analyzed using LC-MS as described below. Standard 24 base DNA oligomers (IDT DNA) containing 0–6 guanine bases were hybridized with their respective complementary strands and diluted to 65 ng  $\mu L^{-1}$  in 50 mM ammonium acetate buffer (pH 6). Fenton reactions were carried out with same DNA concentration with 0.25 M  $\rm H_2O_2$  and 1.5 mM of FeCl $_2$ .for 2 h at 37  $^{\circ}C$ . The solutions were then prepared for LC-MS analysis as described above.

#### 2.7. LC-MS/MS

A SciEx 3200 triple quadrupole LC-MS/MS equipped with a Gemini 3  $\mu m$  NX-C18 110 Å LC column (50  $\times$  2 mm) was used. Two MS detection methods were developed. First, guanine or adenine content was assayed, and second, mass transitions consistent with 8-oxoguanine formation were monitored. For guanine content, analysis was performed in positive ion multiple reaction monitoring (MRM) mode for two mass transitions characterizing fragments of guanine: m/z 152  $\rightarrow$  135, conditions: 150 msec scan time, 36 V declustering potential, 8 V entrance potential, 12 V collision entrance potential, 27 V collision energy, 4 V collision exit cell potential and m/z 152  $\rightarrow$  110, conditions: 150 msec scan time, 36 V declustering potential, 8 V entrance potential, 12 V collision entrance potential, 29 V collision energy, 4 V collision exit cell potential. LC solvents were Solvent A: 0.1% Formic Acid, 95:5 DI H<sub>2</sub>O and Acetonitrile and Solvent B: Methanol. Gradient elution took place via 100% A 0-3 mins, ramp to 75% A mins 3-5. The total analysis time was 5 mins. The flow rate was 0.200 mL min-1 and injection volume was 1.00 µL. Similar protocols for adenine were followed but the monitored mass transitions were m/z 136  $\rightarrow$  119 and 136  $\rightarrow$  92.

For 8-oxo-guanine content, analysis was performed in positive ion MRM mode for two characterizing fragments of 8-oxo-guanine: m/z 158  $\rightarrow$  85, conditions: 150 msec scan time, 16 V declustering potential, 6.5 V entrance potential, 12 V collision entrance potential, 17 V collision energy, 4 V collision exit cell potential and m/z 158  $\rightarrow$  126, conditions: 150 msec scan time, 16 V declustering potential, 6.5 V entrance potential, 12 V collision entrance potential, 11 V collision energy, 4 V collision exit cell potential. LC solvents were A: 0.1% Formic Acid, 98:2 DI  $_{12}$ O and Acetonitrile; B: Methanol; C: Acetonitrile. Gradient elution took place via 45:50:5 A:B:C for 0–1 mins, decreasing A and increasing C by 5%, respectively, for 1–3 mins, holding 35:50:15 A:B:C for 3–4 mins, ramping back to 45:50:5 at 4–6 mins by increasing A and decreasing C by 5%, respectively. Total analysis time was 6 mins. The flow rate was 0.100 mL min-1 and injection volume was 1.00  $\mu$ L.

#### 2.8. Data analysis

Statistical analysis was performed using Excel for MAC 2019, version 16.24 and SCIEX MultiQuant Software, version 3.0. Raw MS and SWV were analyzed using OriginPro 9 software. For SWV plots, background-subtracting was performed using the same SWV electrochemical response for a (PDDA/PSS)2 electrode containing no DNA. Figures were modified using Adobe Illustrator CS6.

## 3. Results

## 3.1. Electrochemical analysis

Our first focus was to monitor DNA extracted from nematodes sourced from different environments. We utilized previously established LbL immobilization and electrochemical protocols to assess the biological DNA samples [21–25,29–32]. Detection takes place via oxidation, and primarily, guanines in the immobilized DNA films are detected on the PG electrodes due to the lower oxidation potential in comparison to other bases [33,34]. The oxidative current is enhanced via an electrocatalytic redox mediator, ruthenium trisbipyridine (Ru(bpy)<sub>3</sub><sup>2+</sup>) [20,21, 29], that is oxidized at the electrode and regenerated by oxidizing

accessible guanines in the DNA according to the following [29,35]:

$$Ru(bpy)_3^{2+} \rightarrow Ru(bpy)_3^{3+} (at electrode)$$
 (1)

$$Ru(bpy)_3^{3+} + G(DNA) \rightarrow G^{\bullet+}(DNA) + Ru(bpy)_3^{2+}$$
 (2)

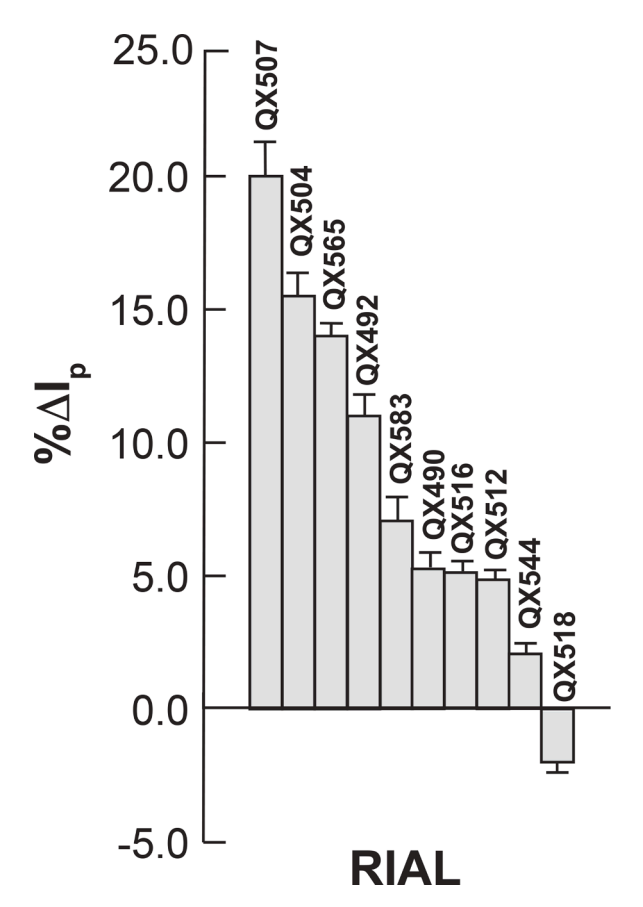
The electrocatalytic signal is heavily dependent on guanine and guanine content in the films. As guanines in the film are damaged, the ruthenium compound can more closely interact with the DNA, which leads to a faster kinetic turnover rate, and higher currents. Therefore, both increases and decrease in  $\rm I_p$  compared to a control state may suggest guanine-related cellular DNA changes [34,36–38]. In our previous report, we showed that exposure to Ni²+ resulted in higher peak currents, and hypothesized that Ni promoted reactive oxygen species (ROS) generation and the formation of 8-oxoG in the nematode DNA [21]. In order to further explore this possibility, additional strains of nematodes from both volcanic and non-volcanic environments were analyzed.

Fig. 1a-b shows a typical background-subtracted SWV response comparison where Ni-exposed nematode extracted DNA was compared to unexposed nematode DNA. The figure shows an oxidation  $\rm I_p$  centered around +1.05 V vs. SCE that is significantly larger in the Ni-exposed sample. Similar current responses were seen in all nematode species and strains where the Ni-exposed samples exhibited higher peak currents. Representative background-subtracted SWV plots for the remaining nematode samples are shown in Figure SI1.

Fig. 1c shows the average peak currents that were detected upon analysis of each of the nematode species and strains within each species. Four nematode DNA samples in total were analyzed. The four DNA samples were sourced one each from two C. elegans and two P. pacificus strains. For each species, one DNA sample derived from a low-nickel environment, Bristol England (C. elegans) or Pasadena, CA (P. pacificus), and one was sourced from volcanic soils with high-nickel exposure, Hawaii (C. elegans) or New Zealand (P. pacificus). Oxidation of DNA from volcanic soil-sourced nematodes resulted in decreased P0 in comparison to the non-volcanic counterparts when exposed to equal concentrations of Ni. This suggests that nematodes originating from environments with continued exposure to Ni may have acquired some genetic protection from accruing DNA damage.

This extends our previous report by demonstrating that we can elucidate how different environments influence the electrochemical DNA oxidation current generated upon analysis. DNA from both species sourced from low-nickel environments, the N2 and P5312 strains of *C. elegans* and *P. pacificus*, respectively, exhibited higher peak currents than the respective volcanic high-nickel sourced strains for the species, CB4856 and RS5696, as those worms were exposed to Ni<sup>2+</sup> due to originating in high-nickel environments. Thus, nickel impacted the DNA of low-nickel sourced nematodes in a more negative manner than the volcanic strains. Those particular strains would have been exposed to very low, if any, concentrations of Ni at their respective source locations and not have been well-adapted to the Ni containing environment examined here [39]. In contrast, nematodes that had evolved in locations of volcanic activity resulting in soil containing higher natural amounts of Ni show some protection from the toxic effects of Ni [40,41].

Based on the results described above, a series of recombinant inbred advanced intercross lines (RIALs) were obtained [28]. The RIALS were formed by crossing parents from N2 and CB4856 *C. elegans* strains. The RIALs were then grown in duplicate cultures one with and one without Ni<sup>2+</sup>, and the DNA was harvested. Here, RIALs were exposed to a higher Ni<sup>2+</sup> concentrations that more accurately model that found in volcanic soil [3]. Extracted DNA was immobilized on PG electrodes and oxidized following similar basic steps as the earlier study (Fig. 1). Fig. 2 shows the peak current percent changes comparing DNA extracted from Ni-exposed worms to that from nonexposed worms. Here, a positive percent change suggests that the Ni-exposed worm DNA exhibited higher I<sub>p</sub> compared to the non-exposed worm DNA. It must be noted that the DNA for this study was ultimately extracted into and adsorbed to the



**Fig. 2.** Average percent  $I_p$  change for denoted RIAL-extracted DNA comparing 0  $\mu$ g  $L^{-1}$  Ni<sup>2+</sup> to 500  $\mu$ g  $L^{-1}$  Ni<sup>2+</sup> exposed responses. Error bars represent s.d. for n=3.

electrode from a higher ionic strength buffer, so the absolute peak current increases or decreases cannot necessarily be interpreted in the same manner as the data seen in Fig. 1. What is clear is that the different RIAL strains exhibit differing resistance to Ni<sup>2+</sup> induced DNA damage based on the wide range of  $\Delta I_p$  exhibited. Generally, Ni<sup>2+</sup> exposed RIAL DNA exhibited larger peak currents suggestive of the accumulation of higher amounts of DNA damage compared to unexposed worms. Further, the RIAL strains varied in their nickel response in a relatively linear fashion, i.e. not a clustered step function. The large  $\Delta I_p$  range suggests that multiple genes are likely involved in protecting the organism from metal toxicity as similar clustered responses would likely be seen across all offspring if protection result of only a few genetic changes in a small number of loci. Interestingly, based on the minimal  $\Delta I_p$  change when comparing DNA extracted from unexposed to Ni-exposed worms, RIALs QX544 and 518 seem to have inherited a combination of genetic loci that endow these organisms with significant protection from Ni-insult.

### 3.2. Mass spectrometry

To understand and explore the DNA changes occurring due to exposure to Ni<sup>2+</sup>, worm-extracted DNA was exposed to acid hydrolysis conditions followed by mass spectrometry (MS) analysis. This technique has been instrumental in providing detailed DNA composition analyses [42–44]. We have previously used similar techniques to validate electrochemical results and determine mutation rates in mice mitochondrial DNA in response to the loss of Brca1 [22]. Similarly, we focused here on both guanine and 8-oxoguanine (8oxoG) due to the importance of this base in the electrochemical analyses.

Fig. 3 shows an initial TOF-MS analysis comparison of hydrolysate from DNA that was extracted from both unexposed (Fig. 3a) and  ${\rm Ni}^{2+}$ 

exposed (Fig. 3b) N2 C. elegans. m/z 152 in both spectra is guanine [M + H], the analysis of which we return to below. The main difference between the two spectra is the emergence of the m/z 158 species from the Ni-exposed sample. Fig. 3c is the product ion spectrum of this m/z 158 species. We had previously suggested that Fenton reaction conditions play a part in the increased oxidative  $I_p$  detected when analyzing nematode DNA based on the ability of  $\mathrm{Ni}^{2+}$  to foster these conditions [21]. We did not find m/z 168 representing 80xoG [M + H] in appreciable quantities in the Ni-exposed sample, but m/z 158 is a known guanidinohydantion rearrangement product of 8xoG. This m/z has been shown to be a more reliable marker of 80xoG formation following hydrolysis [45,46]. The MS/MS spectrum did indeed produce product ions that were indicative of guanidinohydantion formation, and we have previously proposed a fragmentation scheme leading to the observed MS/MS spectrum [22]. Based on this analysis, we monitored the product ion transitions 158→85 and 158→126 to provide relative quantitative analysis of 80xoG formation in the DNA. We have also shown that the presence of this 158→85 or 126 species increases as a function of Fenton condition reaction exposure [22].

Guanine content was quantified from the DNA by monitoring m/z 152 $\rightarrow$ 135 and 152 $\rightarrow$ 110 transitions [22]. Fig. 4a-b shows representative LC-MS/MS chromatograms for the guanine and 80xoG main quantifying transitions from DNA hydrolysis product from unexposed and Ni-exposed worms. The chromatogram peak areas demonstrate that there is a decrease in guanine that is accompanied by an increase in species consistent with 80xoG. This general trend was seen when analyzing the parent nematode strains as well as selected RIALs. These data are summarized in Fig. 4c.

Fig. 4c shows that very little guanine/80xoG differences were detected between DNA samples that had been exposed to 50 or 500 mg  $\rm L^{-1}$   $\rm Ni^{2+}$ . Remaining RIAL DNA was exposed to 500 mg  $\rm L^{-1}$   $\rm Ni^{2+}$  as it more accurately mimics the concentrations seen in volcanic soil [3,47]. The guanine and 80xoG percent changes for these analysis mainly all show that a decrease in guanine is accompanied with a similar increase in 80xoG. This lends additional evidence to ROS generation as the culprit for Ni-induced toxicity. We also monitored adenine content from the N2 and CB strains in the presence or absence of Ni<sup>2+</sup> using a similar methodology as described for guanine. Adenine content was consistent when comparing Ni<sup>2+</sup> exposed to unexposed organisms, and these data are summarized in Table S2. Stable adenine content despite Ni<sup>2+</sup> exposure lends additional evidence that guanine damage leads to In increases and lower guanine content detected upon MS/MS analysis. Accordingly, the RIAL data in Fig. 4 mirror the electrochemical In data shown in Figs. 1 and 2. DNA exhibiting large In increases were accompanied by increased 80xoG content and by extension a decrease in native guanine. However, the data also show some interesting genetic trends from the pairing of the two parental strains. Interestingly, RIAL QX565, which showed a decrease in  $\Delta I_p$  when comparing non-Ni exposed to Ni-exposed DNA, exhibited decreases in both guanine and 80xoG, suggesting additional genetic processes, such as mutation to other bases may be occurring as well. We discuss this possibility below.

## 3.3. 8-oxoguanine content

The MS/MS data show that the decrease in guanine is accompanied with an increase in 80xoG, likely as a result of nickel exposure. In an effort to provide a level of quantitation for 80xoG formation, we created an indirect standard plot based on the guanine MS/MS response.

Double stranded DNA oligomers containing known guanine amounts were acid hydrolyzed before and after exposure to Fenton reaction conditions. LC-MS/MS m/z transitions for both guanine and 80xoG were monitored before and after the Fenton exposure. The difference in guanine detected between undamaged and Fenton-damaged treatments was taken to be the amount of 80xoG generated due to Ni<sup>2+</sup> oxidative damage conditions. The observed m/z 158 $\rightarrow$ 85 LC-MS/MS peak area was then plotted vs. this calculated 80xoG concentration. The linear

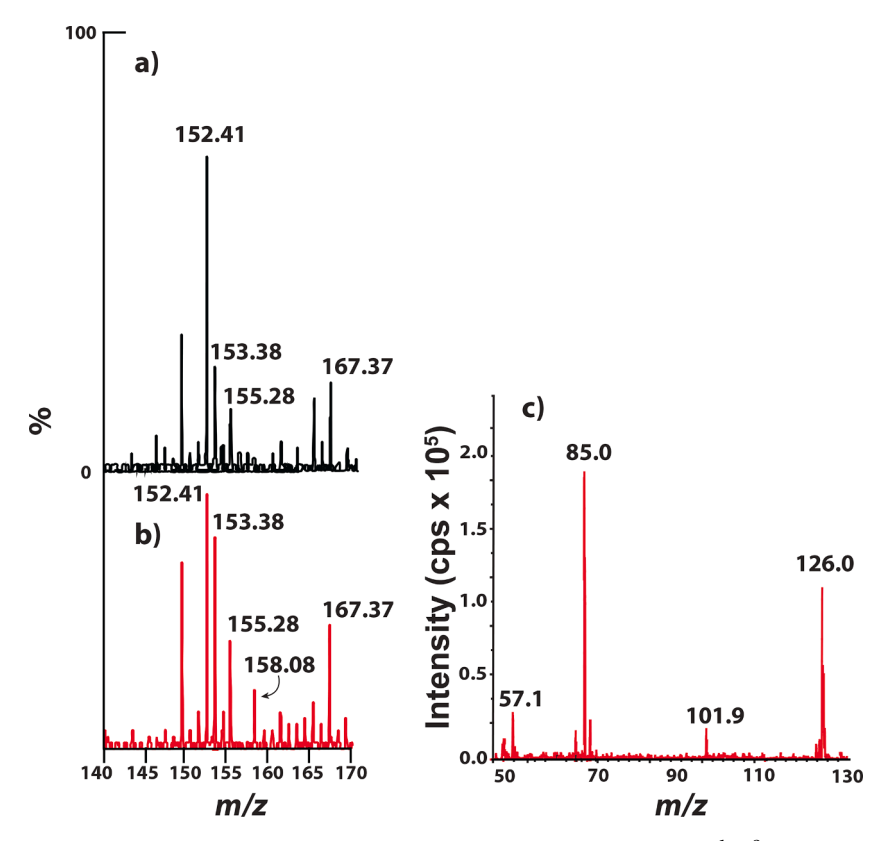
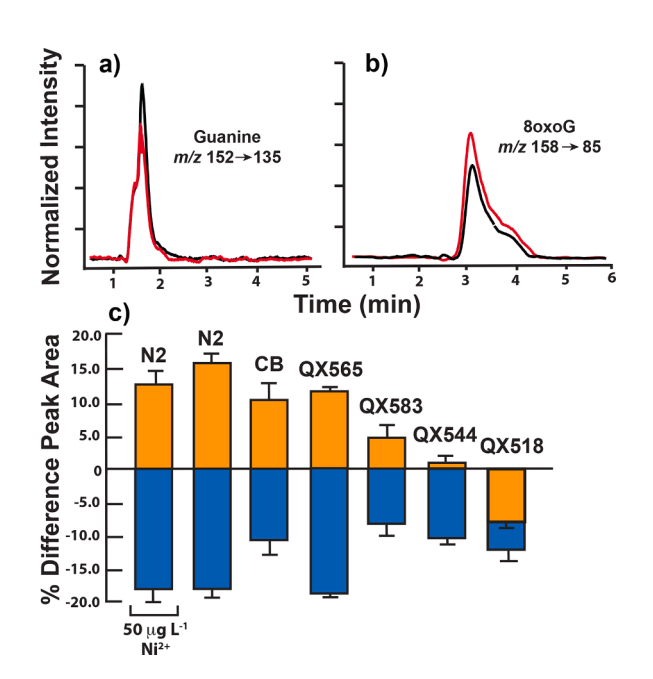


Fig. 3. ESI+ MS spectra of C. elegans extracted hydrolyzed DNA that was exposed to a) 0 or b) 50  $\mu$ g L<sup>-1</sup> Ni<sup>2+</sup>. c) m/z 158 product ion spectrum.



**Fig. 4.** Normalized LC-MS/MS chromatograms monitoring hydrolyed DNA products a) m/z 152  $\rightarrow$  135 and b) m/z 158  $\rightarrow$  85 from N2 nematodes exposed to 0  $\mu$ g L<sup>-1</sup> Ni<sup>2+</sup> (black) or 500  $\mu$ g L<sup>-1</sup> Ni<sup>2+</sup> (red) . Intensity was normalized to starting DNA concentration. c) Average % difference peak area comparison between exposed (500  $\mu$ g L<sup>-1</sup> Ni<sup>2+</sup>or denoted concentration) and non-exposed nematodes for guanine (blue) and 80x0G (orange).

response is shown in Figure S2. Linear regression allowed the means to assign the m/z 158 $\rightarrow$ 85 peak area to an 80xoG concentration upon monitoring the biological DNA samples. Based on the known bp length and GC content of the *C. elegans* genome [48], we were able to calculate

the number of damaged bases detected due to  $\mathrm{Ni}^{2+}$  exposure. The data from this analysis is summarized in Table 1.

Overall, the quantitative data show that nickel induces 80x0G formation in the different RIALS all within the same damage site per guanine magnitude. Negative values for QX518 equate to less detected 80x0G damage for the nickel treatment case. The LC-MS/MS elucidated 80x0G formation frequency is consistent with damage rate findings in other nematode models that looked at base substitution rates in DNA repair mutants [49] and overall 80x0G accumulation to monitor aging impacts [50].

## 4. Discussion

We have previously shown that  $\mathrm{Ni}^{2+}$  unequivocally causes DNA damage. Here, we show that not only does the exposure to  $\mathrm{Ni}^{2+}$  induce DNA damage, but the damage is dependent on the genomic makeup of the nematode strain. Strains collected from nickel-poor environments show a greater susceptibility to damage from nickel exposure than those collected from nickel-rich environments. The electrochemical results in Fig. 1 shows that the  $\mathrm{I}_p$  that is generated after the worms were exposed to

**Table 1** Additional 80xoG detected following  $\mathrm{Ni}^{2+}$ exposure to different *C. elegans* strains.

C. elegans Strain	8oxoG <sup>b</sup>	RSD (%) <sup>c</sup>	80xoG per Guanine <sup>d</sup>
N2	3.53	12.0	0.00763
QX565	2.75	12.1	0.00600
QX585	1.37	15.2	0.00300
QX544	0.71	3.5	0.0015
QX518	-1.50	7.9	-0.00322

 $<sup>^{\</sup>rm a}\,$  80xoG difference between 0 and 500  $\mu g\;L^{-1}\;Ni^{2+}$  exposure.

 $<sup>^{\</sup>rm b}$  ng (ng DNA) $^{-1}$ .

<sup>&</sup>lt;sup>c</sup> n = 3.

<sup>&</sup>lt;sup>d</sup> Calculated based on GC content in C. elegans genome.

Ni $^{2+}$  was lower for worms that were originally from higher volcanic activity soils. It has been extensively shown that the SWV  $I_p$  increases as guanines become more accessible – i.e. as the DNA is damaged – therefore, the lower  $I_p$  seen for the volcanic Ni-exposed worms suggests less guanine damage in those DNA extracts. The MS/MS data suggest that this is consistent with lower amounts of Ni-related ROS damage. The volcanic soils in which these worms were sourced are known to contain over 500  $\mu g \ mL^{-1}$  nickel. Therefore, these data are consistent with nematodes residing in the volcanic soils/environs adapting to these conditions and evolving protective mechanisms to counteract Ni-induced toxicity that are inherited through the genome.

These genetic considerations were further seen in the RIAL analysis (Fig. 2). The electrochemical I<sub>p</sub> data show that non-volcanic soil (N2) and volcanic soil (CB) parents produced RIAL strains exhibiting a wide range of DNA damage in response to Ni<sup>2+</sup> exposure. The linear range of RIAL  $\Delta I_p$  suggest that multiple genes are involved in the Ni<sup>2+</sup> response adaptation, which putatively involves protein complexes and sophisticated genetic regulatory circuits [51-54]. The observed In differences represent molecular and genetic differences in these mechanisms contributing to differing nickel susceptibility. In order to potentially identify the specific genes involved, further RIALs must be tested and full quantitative trait loci analyses must be performed. However, even amongst the electrochemically screened RIALs already tested, some exhibited very limited DNA Ip increases (QX 544) or even decreases (QX 518) upon Ni<sup>2+</sup> exposure. These RIALs represent an initial starting point to begin further development of hundreds of RIALs to fully understand the genetic mechanisms involved in nickel toxicity protection.

The mass spectrometry findings complement the electrochemical data by showing that the SWV  $\rm I_p$  increases are likely due to the formation of 80xoG due to Ni²+ exposure. A decline in guanine content in Ni²+ exposure samples was detected in both parent strains and RIALs. This decrease was typically accompanied with similar levels of increase in m/z species consistent with 80xoG formation in the DNA. These data are consistent with the conversion of guanine to 80xoG in the DNA due to Ni²+ exposure, leading to the increased SWV  $\rm I_p$ . Further supporting our previous findings hypothesizing that ROS likely led to the increased  $\rm I_p$  for DNA that had originated from Ni²+ exposed worms.

The increases in 80xoG content do not completely mirror the guanine content losses, as the 80xoG increases are typically not as high as guanine loss. This is clearly evident in the RIALs that exhibit lower or negative  $I_p$  comparisons upon  $\mathrm{Ni}^{2+}$  exposure. This suggests additional genetic or chemical processes occur to the guanine bases upon  $\mathrm{Ni}^{2+}$  exposure. While N2 and CB strains exhibited consistent adenine content despite  $\mathrm{Ni}^{2+}$  exposure (Table S2), one possibility is that 80xoG formation could lead to point mutations. It has been shown that the conversion from G $\rightarrow$ A occurs in worms due to ROS induced damage [55,56]. This could also explain the loss of guanine in the QX 544 and 518 RIALs without the concomitant increase in 80xoG. Future MS analyses will be performed to explore this possibility.

## 5. Conclusion

Overall, we have used an electrochemical platform to rapidly analyze DNA from live animals to study environmental genetic adaption to toxic heavy metal insult. DNA extracted from nickel-exposed nematode strains that originated in soils/environs where nickel was more prevalent exhibited lower amounts of damage compared to that from nematodes strains from non-volcanic low-nickel soils/environs. This suggests an enhanced ability of the adapted worms to protect themselves from genetic damage upon metal exposure. Complementary tandem MS analysis showed that the SWV peak current increases are likely due to guanine content decrease accompanied with 80x0G formation in the DNA. Furthermore, RIAL strains derived from a genetic cross between non-volcanic and volcanic derived parent strains exhibited a wide range of SWV I<sub>p</sub> upon DNA analysis suggesting a complex genetic and biochemical mechanism involved in the toxicity protection. MS analysis

showed that RIAL strains that were more resistant to  ${\rm Ni}^{2+}$  damage as monitored using SWV exhibited less 80xoG content compared to RIAL strains exhibiting elevated  ${\rm I}_{\rm p}$  upon  ${\rm Ni}^{2+}$  exposure. Results presented here show that an electrochemical platform and complementary MS analysis can provide insight into a complicated environmental genetic adaptation mechanism.

#### **Declaration of Competing Interest**

The authors declare that they have no known competing financial interests or personal relationships that could have appeared to influence the work reported in this paper.

#### Supplementary materials

Supplementary material associated with this article can be found in the online version at doi:10.1016/j.snr.2021.100070.

#### References

- D. Rudel, C.D. Douglas, I.M. Huffnagle, J.M. Besser, C.G. Ingersoll, Assaying environmental nickel toxicity using model nematodes, PLoS ONE 8 (2013) e77079.
- [2] G. Genchi, A. Carocci, G. Lauria, M.S. Sinicropi, A. Catalano, Nickel: human health and environmental toxicology, IJERPH 17 (2020) 679.
- [3] Y.A. Iyaka, Nickel in soils: a review of its distribution and impacts, SRE 6 (2011) 6774–6777.
- [4] M. Saito, R. Arakaki, A. Yamada, T. Tsunematsu, Y. Kudo, N. Ishimaru, Molecular Mechanisms of Nickel Allergy, Int. J. Mol. Sci. 17 (2016) 202, https://doi.org/ 10.3390/ijms17020202.
- [5] L. Macomber, R.P. Hausinger, Mechanisms of nickel toxicity in microorganisms, Metallomics 3 (2011) 1153–1162.
- [6] H. Guo, L. Chen, H. Cui, X. Peng, J. Fang, Z. Zuo, J. Deng, X. Wang, B. Wu, Research advances on pathways of nickel-induced apoptosis, Int. J. Mol. Sci. 17 (2016) 10.
- [7] R. Eisler, Nickel hazards to fish, wildlife, and invertebrates: a synoptic review, Biol. Sci. Rep. 34 (1998).
- [8] M. Alfano, C. Cavazza, Structure, function, and biosynthesis of nickel-dependent enzymes, Protein Sci 29 (2020) 1071–1089.
- [9] C.J. Riger, P.N. Fernandes, L.F. Vilela, A.A. Mielniczki-Pereira, D. Bonatto, J.A. P. Henriques, E.C.A. Eleutherio, Evaluation of heavy metal toxicity in eukaryotes using a simple functional assay, Metallomics 3 (2011) 1355–1361.
- [10] K.-i. Tanaka, M. Kasai, M. Shimoda, A. Shimizu, M. Kubata, M. Kawahara, Nickel enhances zinc-induced neuronal cell death by priming the endoplasmic reticulum stress response, Oxid. Med. Cell. Long. 2019 (2019) 1–13.
- [11] F.W. Sunderman Jr, R.M. Maenza, P.R. Alpass, J.M. Mitchell, I. Damjanov, P. J. Goldblatt, Carcinogenicity of nickel subsulfide in Fischer rats and Syrian hamsters after administration by various routes, Adv. Exp. Med. Biol. 91 (1977) 57-67
- [12] Y. Chervona, A. Arita, M. Costa, Carcinogenic metals and the epigenome: understanding the effect of nickel, arsenic, and chromium, Metallomics 4 (2012) 619–627
- [13] L.M. Falcone, A. Erdely, R. Salmen, M. Keane, L. Battelli, V. Kodali, L. Bowers, A. B. Stefaniak, M.L. Kashon, J.M. Antonini, P.C. Zeidler-Erdely, Pulmonary toxicity and lung tumorigenic potential of surrogate metal oxides in gas metal arc welding-stainless steel fume: iron as a primary mediator versus chromium and nickel, PLoS ONE 13 (2018), e0209413.
- [14] N. Saul, S. Möller, F. Cirulli, A. Berry, W. Luyten, G. Fuellen, Health and longevity studies in C. elegans: the "healthy worm database" reveals strengths, weaknesses and gaps of test compound-based studies, Biogerontology 22 (2021) 215–223.
- [15] H.A. Tissenbaum, Using C. elegans for aging research, Invertbr. Reprod. Dev. 59 (2015) 59–63.
- [16] M. Munasinghe, A. Abdullah, J. Thomas, D. Heydarian, M. Weerasinghe, M. Jois, Cocoa improves age-associated health and extends lifespan in C. elegans, J. Nutr. Health Aging 6 (2021) 73–86.
- [17] S. Alarifi, D. Ali, S. Alakhtani, E.S. Al Suhaibani, A.A. Al-Qahtani, Biol. Trace Elem. Res. 157 (2014) 84–93.
- [18] B. Conradt, D. Xue, Programmed cell death, Wormbook (2005) 1-13.
- [19] P.M. Mangahas, Z. Zhou, Clearance of apoptopic cells in Caenorhabditis elegans, Semin. Cell Dev. Biol. 16 (2005) 295–306.
- [20] K. Cai, C. Ren, Z. Yu, Nickel-induced apoptosis and relevant signal transduction pathways in Caenorhabditis elegans, Toxicol. Ind. Health 26 (2010) 249–256.
- [21] I.M. Huffnagle, A. Joyner, B. Rumble, S. Hysa, D. Rudel, E.G. Hvastkovs, Dual electrochemical and physiological apoptosis assay detection of in vivo generated nickel chloride induced DNA damage in caenorhabditis elegans, Anal. Chem. 86 (2014) 8418–8424.
- [22] E.R. LaFave, M.D. Tarpey, N.P. Balestrieri, E.E. Spangenburg, E.G. Hvastkovs, Complementary square-wave voltammetry and LC-MS/MS analysis to elucidate induced damaged and mutated mitochondrial and nuclear DNA from in-vivo knockdown of the BRCA1 gene in the mouse skeletal muscle, Anal. Chem. 93 (2021) 11592–11600.

- [23] A. Mugweru, J.F. Rusling, Square wave voltammetric detection of chemical DNA damage with catalytic poly(4-vinylpyridine)-Ru(bpy)22+ films, Anal. Chem. 74 (2002) 4044–4049.
- [24] J. Mbindyo, L. Zhou, Z. Zhang, J.D. Stuart, J.F. Rusling, Detection of chemically-induced DNA damage by derivative square-wave voltammetry, Anal. Chem. 72 (2000) 2059–2065.
- [25] J.F. Rusling, Sensors for toxicity of chemicals and oxidative stress based on electrochemical catalytic DNA oxidation, Biosens. Bioelectron. 20 (2004) 1022–1028
- [26] M.V. Rockman, L. Kruglyak, Breeding designs for recombinant inbred advanced intercross lines, Genetics 179 (2008) 1069–1078.
- [27] M.V. Rockman, L. Kruglyak, Recombinational landscape and population genomics of Caenorhabditis elegans, PLoS Genet. 5 (2009), e1000419.
- [28] E.C. Andersen, T.C. Shimko, J.R. Crissman, R. Ghosh, J.S. Bloom, H.S. Seidel, J. P. Gerke, L. Kruglyak, A powerful new quantitative genetics platform, combining caenorhabditis elegans high-throughput fitness assays with a large collection of recombinant strains, G3 (Bethesda) 13 (2015) 911–920, https://doi.org/10.1534/g3.115.017178.
- [29] S.M. Silva, R. Tavallaie, V.R. Gonçales, R.H. Utama, M.B. Kashi, D.B. Hibert, R. D. Tilley, J.J. Gooding, Dual signaling DNA electrochemistry: an approach to understand DNA interfaces, Langmuir 34 (2018) 1249–1255.
- [30] E.E. Ferapontova, DNA electrochemistry and electrochemical sensors for nucleic acids, Annu. Rev. Anal. Chem. (Palo Alto Calif) 11 (2018) 197–218.
- [31] J.I.A. Rashid, N.A. Yusof, The strategies of DNA immobilization and hybridization detection mechanism in the construction of electrochemical DNA sensor: a review, Sens. Biosensing Res. 16 (2017) 19–31.
- [32] W.G. Kuhr, Electrochemical DNA analysis comes of age, Nat. Biotechnol. 18 (2000) 1042–1043
- [33] A. Brett, Electrochemistry for Probing DNA Damage, in: C.A. Grimes, E.C. Dickey and M.V. Pishko (Eds.), Encyclopedia of Sensors Vol. X, American Scientific Publishers, Stevenson Ranch, C.A., 2006, p. 1–14.
- [34] H. Xiong, Y. Chen, X. Zhang, H. Gu, S. Wang, An electrochemical biosensor for the rapid detection of DNA damage induced by xanthine oxidase-catalyzed Fenton reaction, Sens. Actuators B 181 (2013) 85–91.
- [35] D.H. Johnson, K.C. Glasgow, H.H. Thorp, Electrochemical measurement of the solvent accessibility of nucleobases using electron transfer between DNA and metal complexes, J. Am. Chem. Soc. 117 (1995) 8933–8938.
- [36] Y. Wang, H. Xiong, X. Zhang, S. Wang, Electrochemical biosensors for the detection of oxidative DNA damage induced by Fenton reagents in ionic liquid, Sens. Actuat. B 161 (2012) 274–278.
- [37] C. Lü, T.-F. Kang, L.-P. Lu, Y. Xiong, Electrochemical DNA sensors for rapid detection of DNA damage induced by fenton reaction, Chinese J. Anal. Chem. 40 (2012) 1822–1826.
- [38] R.P. Bowater, R.J.H. Davies, E. Alecek, M. Fojta, Sensitive electrochemical assays of DNA structure: electrochemical analysis of DNA, Chim-Oggi Chem. Today 27 (2009) 50–54.
- [39] R. McSorley, Adaptations of nematodes to environmental extremes, Florida Entomol. Soc. 86 (2003) 138–142.
- [40] Hawaiian Islands Soil Metal Background Evaluation Report, 19, Hawai'i Dept. of Health, 2012.

- [41] Background Concentrations of Inorganic Elements in Soils from the Auckland Region, ARC Technical Publication No. 153, 2002.
- [42] P. Cheng, Y. Li, S. Li, M. Zhang, Z. Zhou, Collision-induced disassociation (CID) of guanine radical cation in the gas phase: an experimental and computational study, Phys. Chem. Chem. Phys. 12 (2010) 4667–4677.
- [43] L. Sadr-Arani, P. Mignon, H. Chermette, H. Abdoul-Carime, B. Farizon, M. Farizon, Fragmentation mechanisms of cytosine, adenine and guanine ionized bases, Phys. Chem. Chem. Phys. 17 (2015) 11813–11826.
- [44] I.I. Shafranyosh, Y.Y. Svida, M.I. Sukhoviya, M.I. Shafranyosh, B.F. Minaev, G. V. Baryshinkov, V.A. Minaeva, Absolute effective cross sections of ionization of adenine and guanine molecules by electron impact, Tech. Phys. 60 (2015) 1430–1436.
- [45] S.G. Swarts, G.S. Smith, L. Miao, K.T. Wheeler, Effects of formic acid hydrolysis on the quantitation of radiation-induced DNA base damage products by gas chromatography/mass spectrometry, Radiat. Environ. Biophys. 35 (1996) 41–53.
- [46] M.C. Kelley, G. Whitaker, B. White, M.R. Smyth, Nickel (II)-catalysed oxidative guanine and DNA damage beyond 8-oxoguanine, Free Radic. Biol. Med. 42 (2007) 1680–1689.
- [47] M. Van Mouwerk, L. Stevens, D.B. Seese, W. Basham, R.J. Irwin, Environmental contaminants encyclopedia, Nat. Park Serv. (1997).
- [48] T. Blumenthal, D. Evans, C.D. Link, A. Guffanti, D. Lawson, J. Thierry-Mieg, D. Thierry-Mieg, W.L. Chiu, K. Duke, M. Kiraly, S.K. Kim, A global analysis of Caenorhabditis elegans operons, Nature 417 (2002) 851, https://doi.org/10.1038/ nature00831.
- [49] B. Meier, N. Volkova, Y. Hong, S. Bertolini, V. Gonzàlex-Huici, T. Petrova, S. Boulton, P.J. Campbell, M. Gerstung, A. Gartner, Protection of the C. elegans germ cell genome depends on diverse DNA repair pathways during normal proliferation, PLoS ONE 16 (2021), e0250291.
- [50] L.H.H. Aung, Y. Wang, Z.-Q. Liu, Z. Li, Z. Yu, X. Chen, J. Gao, P. Shan, Z. Zhou, P. Li, Agewise mapping of genomic oxidative DNA modification demonstrates oxidative-driven reprogramming of pro-longevity genes, BioRxiv (2020), https://doi.org/10.1101/2020.02.17.951582.
- [51] I. Cleynen, J. Halfvarsson, How to approach understanding complex trait genetics—Inflammatory bowel disease as a model complex trait, United Eur. Gastroent. 7 (2019) 1426–1430.
- [52] S. Nogami, Y. Ohya, G. Yvert, Genetic complexity and quantitative trait loci mapping of yeast morphological traits, PLOS Genet. 3 (2007) e31.
- [53] A. Burga, E. Ben-David, T.L. Vergara, J. Boocock, L. Kruglyak, Fast genetic mapping of complex traits in C. elegans using millions of individuals in bulk, Nat. Commun. 10 (2019) 2680.
- [54] T. Sugi, Genome editing in C. elegans and other nematode species, Int. J. Mol. Sci. 17 (2016) 295.
- [55] D.R. Denver, L.J. Wilhelm, D.K. Howe, K. Gafner, P.C. Dolan, C.F. Baer, Variation in base-substitution mutation in experimental and natural lineages of Caenorhabditis nematodes. GBE 4 (2012) 513–522.
- [56] Y. Sanada, Q.-.M. Zhang-Akiyama, An increase of oxidised nucleotides activates DNA damage checkpoint pathway that regulates post-embryonic development in Caenorhabditis elegans, Mutagenesis 29 (2014) 107–114.